



CHORUS

This is the accepted manuscript made available via CHORUS. The article has been published as:

Phonon thermodynamics and elastic behavior of GaN at high temperatures and pressures

Jane E. Herriman, Olle Hellman, and Brent Fultz

Phys. Rev. B **98**, 214105 — Published 6 December 2018

DOI: [10.1103/PhysRevB.98.214105](https://doi.org/10.1103/PhysRevB.98.214105)

Phonon thermodynamics and elastic behavior of GaN at high temperatures and pressures

Jane E. Herriman,¹ Olle Hellman,^{1,2} and Brent Fultz¹

¹*Department of Applied Physics and Materials Science,
California Institute of Technology, Pasadena, California 91125, USA*

²*Department of Physics, Chemistry and Biology (IFM), Linköping University, SE-581 83 Linköping, Sweden*

The effects of temperature and pressure on the phonons of GaN were calculated for both the wurtzite and zincblende structures. The quasiharmonic approximation (QHA) gave reasonable results for the temperature dependence of the phonon DOS at zero pressure, but unreliably predicted the combined effects of temperature and pressure. Pressure was found to change the explicit anharmonicity, altering the thermal shifts of phonons, and more notably qualitatively changing the evolution of phonon lifetimes with increasing temperature. These effects were largest for the optical modes, and phonon frequencies below approximately 5 THz were adequately predicted with the QHA.

The elastic anisotropies of GaN in both wurtzite and zincblende structures were calculated from the elastic constants as a function of pressure at 0 K. The elastic anisotropy increased with pressure until reaching elastic instabilities at 40 GPa (zincblende) and 65 GPa (wurtzite). The calculated instabilities are consistent with proposed transformation pathways to rocksalt GaN, and place upper bounds on the pressures at which wurtzite and zincblende GaN can be metastable.

I. INTRODUCTION

GaN is a wide-band-gap semiconductor used in optoelectronic devices such as light-emitting diodes (LEDs). Under ambient conditions GaN adopts the wurtzite structure, composed of two interpenetrating hexagonal close-packed lattices of Ga and N atoms. Like other III-V materials, GaN is polytypic, and zincblende GaN is metastable at ambient conditions (see Fig. 1). The zincblende structure consists of interpenetrating face-centered cubic lattices, differing from the wurtzite structure only in the relative positioning of ionic planes; wurtzite has ABABAB... stacking; zincblende has ABCABC... stacking.¹ Zincblende GaN is technologically relevant because its metastability allows it to be grown under ambient conditions,² and it is more easily doped than wurtzite GaN.³

At elevated pressures, III-V materials tend to transform to either the β -Sn structure for more covalent compounds or the rocksalt structure for more ionic compounds.⁴ With pressure GaN transforms to the rocksalt structure, changing from tetrahedral to octahedral coordination. Calculations and measurements show that

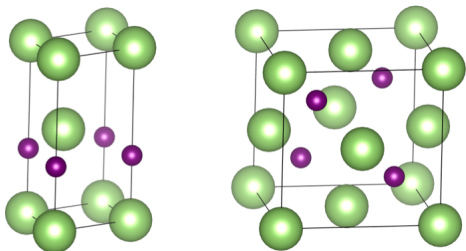


FIG. 1: Unit cells of the wurtzite (left) and zincblende (right) structures, with underlying hexagonal and cubic lattices.

the transformation pressure in GaN is between 30 and 50 GPa.^{4,5} There has been much discussion in the literature of the transformation pathway from the wurtzite to rocksalt structure, resulting in a consensus that GaN adopts an intermediate tetragonal structure.^{1,6-8}

Calculations of thermodynamic functions at elevated temperatures are a greater challenge than calculations at elevated pressures. The quasiharmonic approximation (QHA) is a common approach, where the effects of temperature on the phonon frequency ω_i are included through the thermal expansion β , and the mode Grüneisen parameter γ_i (Eq. 3). In a QHA the harmonic nature of the phonons is preserved. Since harmonic phonons do not interact, they have infinite lifetimes and the thermal conductivity is infinite. The potential energy surface of a crystal does not vary with temperature in a QHA. The QHA assumes that all effects of temperature originate from changes in volume, with phonons having the same response as from pressure. A QHA therefore ignores explicit anharmonicity from phonon-phonon interactions caused by cubic or quartic perturbations to the potential energy. These explicit anharmonic effects can be important even at low temperatures, however, and typically grow with temperature. Explicit anharmonicity can alter thermal expansion,⁹ elastic anisotropy,¹⁰ phase stability,¹¹ and, of course, transport properties.¹¹ It is not yet well understood when the QHA is adequate, or if it can be extended to better include anharmonic effects. One useful test is if the accuracy of the QHA varies with pressure.

The present study reports an investigation of phonon frequencies and lifetimes in wurtzite and zincblende GaN as functions of temperature and pressure, and elastic anisotropy as a function of pressure. The methods and results are described in Sections II and III. After first discussing effects of pressure at 0 K and of temperature at 0 GPa, it is shown that the effects of T and P on phonons

are not additive, and for phonon linewidths there is a marked interdependence of effects from T and P . We also report that the elastic anisotropy increases with pressure in both wurtzite and zincblende GaN, until each structure reaches an elastic instability at 40 and 65 GPa, respectively. Section IV discusses the explicit anharmonicity and the reliability of a QHA for phonon properties, and how the elastic anisotropy gives upper bounds on the pressures at which wurtzite and zincblende GaN can persist as thermodynamically metastable phases (when rocksalt GaN is the equilibrium structure).

II. COMPUTATIONAL

Ab initio calculations were performed on GaN using density functional theory¹² (DFT) as implemented in the Vienna Ab-initio Simulation Package^{13,14} (VASP), using a projector augmented wave method¹⁵, the local density approximation (LDA), and a plane wave cutoff of 600 eV. Total energies and elastic constants were calculated for static lattices using a two-atom zincblende primitive unit cell and a four-atom wurtzite primitive unit cell with $22 \times 22 \times 22$ and $20 \times 20 \times 12$ k -point meshes, respectively. For phonon calculations, $4 \times 4 \times 4$ and $5 \times 5 \times 4$ k -point meshes were used for zincblende and wurtzite supercells with 216 and 192 atoms, respectively. All k -point meshes were generated with a Monkhorst-Pack scheme¹⁶.

Helmholtz free energies, $F(V, T)$, were calculated as

$$F(V, T) = E_0(V) + F_{\text{ph}}(V, T), \quad (1)$$

where $E_0(V)$ is the ground state total energy from VASP as a function of volume and $F_{\text{ph}}(V, T)$ is the phonon free energy at a particular volume and temperature. Finite temperature phonon properties were calculated using a version of the temperature dependent effective potential method TDEP.^{17–19} This version, s-TDEP, was stochastically-initialized,²⁰ and accounted for zero point motion. In brief, ensembles of supercells were populated with atoms that were given thermal displacements with phonon populations and polarizations from a quasiharmonic model, and the ensemble average of the energies was used to obtain the best “effective potential” of the form

$$H = U_0 + \sum_i \frac{\mathbf{p}_i^2}{2m} + \frac{1}{2} \sum_{ij\alpha\beta} \Phi_{ij}^{\alpha\beta} u_i^\alpha u_j^\beta + \frac{1}{3!} \sum_{ijk\alpha\beta\gamma} \Phi_{ijk}^{\alpha\beta\gamma} u_i^\alpha u_j^\beta u_k^\gamma. \quad (2)$$

Optimized $\Phi_{ij}^{\alpha\beta}$ and $\Phi_{ijk}^{\alpha\beta\gamma}$ were obtained by minimizing the differences between the forces on the atoms in the ensemble and the forces obtained from the effective potential of Eq. 2. (The concept of an effective potential for phonons dates back many years and is reviewed in a delightful paper by Klein and Horton,²¹ (also Hooton²²),

who explained in detail how the quartic term in the potential renormalizes the quadratic term in Eq. 2.) Force constant determinations account for long range interactions in polar materials that generate LO-TO splitting using Gonze and Lee’s correction scheme^{23,24} and VASP Born effective charge tensors.

Phonon properties were calculated for wurtzite and zincblende GaN at 0 and 1120 K at each of three pressures: 0, 30, and 60 GPa in wurtzite GaN and 0, 15, and 30 GPa in zincblende GaN (pressures confirmed to be within their ranges of elastic stability). To determine equilibrium material structures at these pressures and temperatures, Helmholtz free energies, $F(V, T)$, were calculated for each material and temperature as a function of volume. Free energies were evaluated only at volumes within the regime of elastic stability in each material; the free energy was evaluated at 14 volumes corresponding to pressures below 64 GPa in wurtzite GaN and at 10 volumes corresponding to pressures below 36 GPa in zincblende GaN. These energy-volume relationships were fitted with a Birch-Murnaghan equation of state to determine pressure as a function of volume at fixed temperature. Pressures and temperatures of interest were then evaluated by computing phonon properties on supercells of wurtzite and zincblende GaN held at the corresponding volumes. In wurtzite GaN, aspect ratios were determined quasiharmonically by relaxing a unit cell of wurtzite GaN at volumes of interest with ground state DFT.

III. RESULTS

A. Phonon property calculations

1. Temperature effects

Figure 2 shows phonon densities of states (DOS) for the zincblende and wurtzite structures at 0 GPa. The phonons at 1120 K were calculated in two ways. The dotted curves labeled “QHA 1120K” were calculated for harmonic force constants with the equilibrium volumes for 1120 K, and a 0 K effective potential. The red curves “1120K” were calculated with force constants from the s-TDEP method, and include effects of both volume expansion and explicit anharmonicity. Comparing the phonon DOS “1120K” with “QHA 1120K” shows the effect of explicit anharmonicity. Evidently, the QHA gives a reasonable temperature dependence of the phonon DOS at 0 GPa. Figure 3 gives a more detailed look at how individual phonon dispersions shift with temperature. We see that while phonon frequency shifts occur for higher frequency phonon modes (as evidenced by offsets between blue and red curves), phonon frequencies of acoustic modes near the Γ point do not appear to change between 0 and 1120 K in either material, consistent with the phonon DOS of Fig. 2. Figure 4 shows again the phonon dispersions at 0 GPa for wurtzite and zincblende GaN at

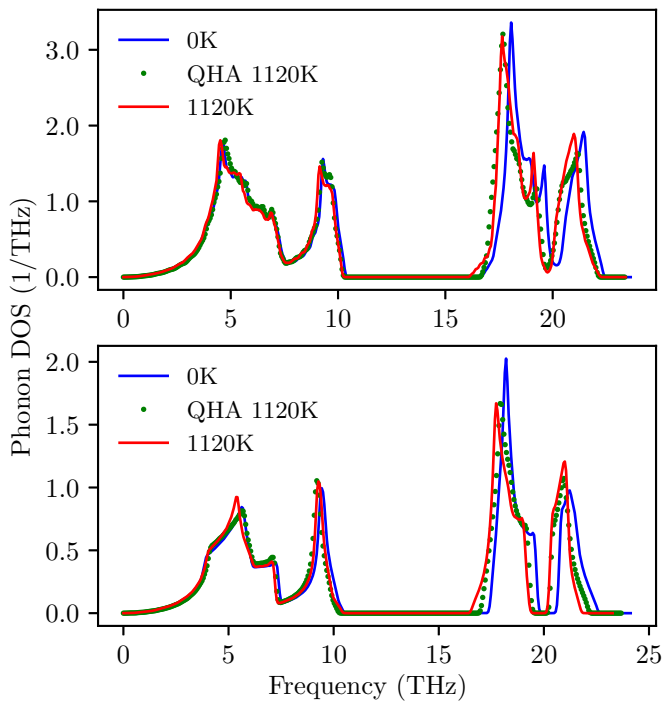


FIG. 2: Phonon DOS at 0 GPa for wurtzite (top) and zincblende (bottom) GaN at 0 K (blue), at 1120 K by the QHA (green dots), and at 1120 K by s-TDEP (red).

0 and 1120 K, now overlaid with phonon linewidth information. There is a substantial broadening of the optical modes at 1120 K, which comes from reduced phonon lifetimes in s-TDEP.

2. Pressure effects

Figure 5 shows the effects of pressure on the phonon DOS of the zincblende and wurtzite structures at 0 K. (The Supplemental Information shows that the pressure-driven changes of the phonon DOS are qualitatively similar at 1120 K.) Above approximately 6 THz, phonon modes stiffen with increasing pressure, but below this frequency the phonons soften.

Mode Grüneisen parameters γ_i are defined as

$$\gamma_i = -\frac{V}{\omega_i} \frac{\partial \omega_i}{\partial V}, \quad (3)$$

The γ_i are commonly positive, so phonon stiffening is expected with increasing pressure. (In contrast, systems that exhibit negative thermal expansion have one or more mode Grüneisen parameters that are negative.) The mixture of phonon softening and stiffening with increasing pressure seen in Fig. 5, is reflected in Fig. 6 for

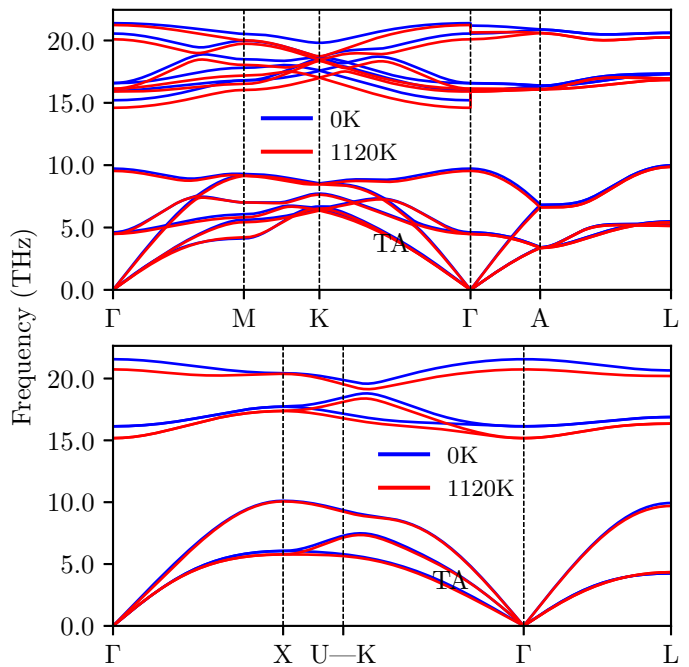


FIG. 3: Phonon dispersions at 0 GPa for wurtzite (top) and zincblende (bottom) GaN at 0 K (blue) and 1120 K (red). TA denotes the transverse acoustic branches.

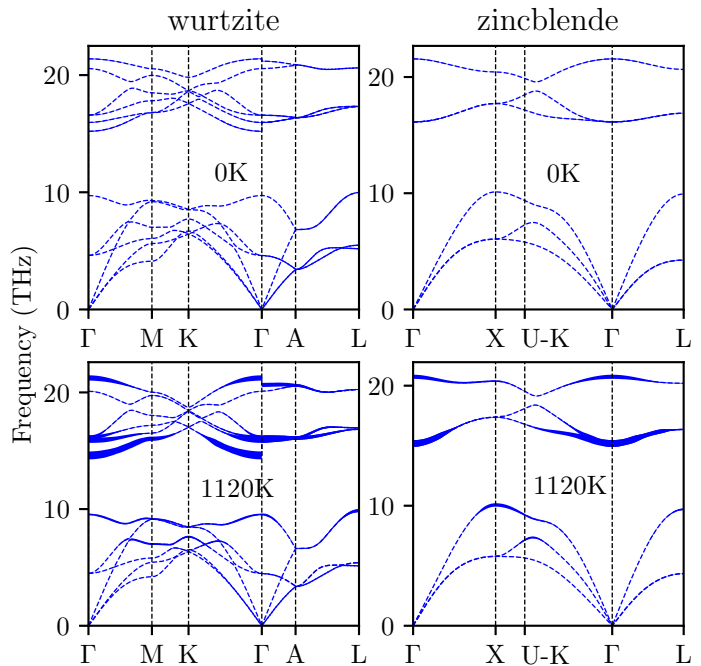


FIG. 4: Phonon dispersions at 0 GPa for wurtzite (left) and zincblende (right) GaN at 0 K (top) and 1120 K (bottom) vs. \mathbf{k} along different directions in the Brillouin zone. Line thicknesses indicate the phonon linewidths, showing broadening of phonon modes at 1120 K.

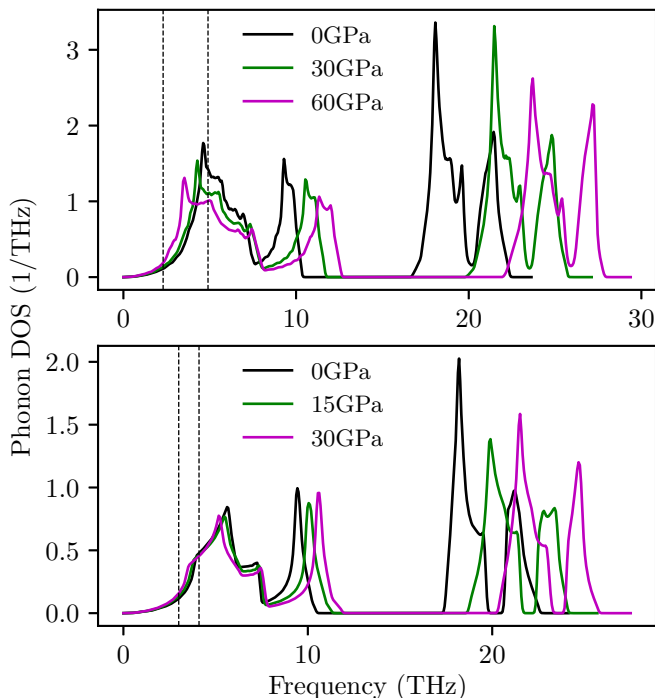


FIG. 5: Phonon DOS at 0K for wurtzite GaN at 0, 30, and 60 GPa (top), and for zincblende GaN at 0, 15, and 30 GPa (bottom). Acoustic modes below 6 THz exhibit softening with increased pressure, whereas higher energy modes stiffen. Dashed vertical black lines delineate a feature in the DOS that softens with increasing pressure.

mode Grüneisen parameters at 0K for three pressures. The Grüneisen mode parameters of the transverse acoustic branches are negative for both structures of GaN, consistent with negative Grüneisen parameters for transverse acoustic modes reported in both the zincblende^{25–27} and wurtzite structures.^{7,8} The Grüneisen parameters for most other modes, including optical modes, are not large.

Figure 6 shows that the negative mode Grüneisen parameters become more negative with increasing pressure. A consequence is seen between the vertical black dashed lines in Fig. 5 – the leftward phonon frequency shift from the green to pink curves is greater than that from the black to green curves. In zincblende GaN, the increase of 15 GPa from 15 to 30 GPa causes the phonon frequencies to decrease more than does the increase of 15 GPa from 0 to 15 GPa. In wurtzite GaN, the increase of 30 GPa from 30 to 60 GPa shifts the phonon frequencies obviously more than the same pressure increase between 0 and 30 GPa.

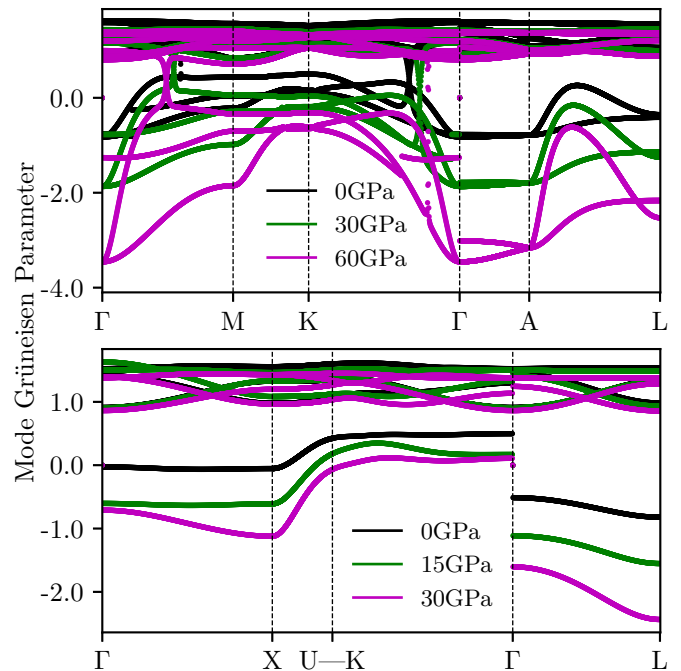


FIG. 6: Mode Grüneisen parameters at 0K for all phonon branches at three pressures in wurtzite (top) and zincblende (bottom). In both panels, pressure increases from the black to green to pink. Pressure causes large changes in the negative Grüneisen parameters, which correspond to transverse acoustic modes.

3. Coupled temperature-pressure effects

Figure 8 shows an overlay of the 1120 K phonon DOS curves at 0 GPa with rescaled DOS curves from 30 GPa. Specifically, the 30 GPa DOS was rescaled linearly in frequency so its first moment is the same as the DOS at 0 GPa. This rescaling reveals changes in the shape of the DOS with pressure. These changes alter the intrinsic anharmonicity, as discussed later.

Figure 9 shows thermal broadenings of phonon linewidths for three pressures. The largest phonon broadenings occur near the Γ point for both structures of GaN, but these thermal broadenings change considerably with pressure.

The effects of pressure on the thermal broadening are markedly different for the different phonons – the shapes of the curves at 0 GPa are not simply rescaled with pressure. Furthermore, for individual phonons the effects of pressure are highly nonlinear. For example, the thermal broadenings of phonons near the Γ point of both structures are reduced by the first increase in pressure (from 0 to 30 GPa in wurtzite and from 0 to 15 GPa in zincblende GaN), but for most phonons the reduction of thermal broadening is much greater as the pressure increases again, from 30 to 60 GPa in wurtzite GaN and from 15 to 30 GPa in zincblende GaN. Curiously, the

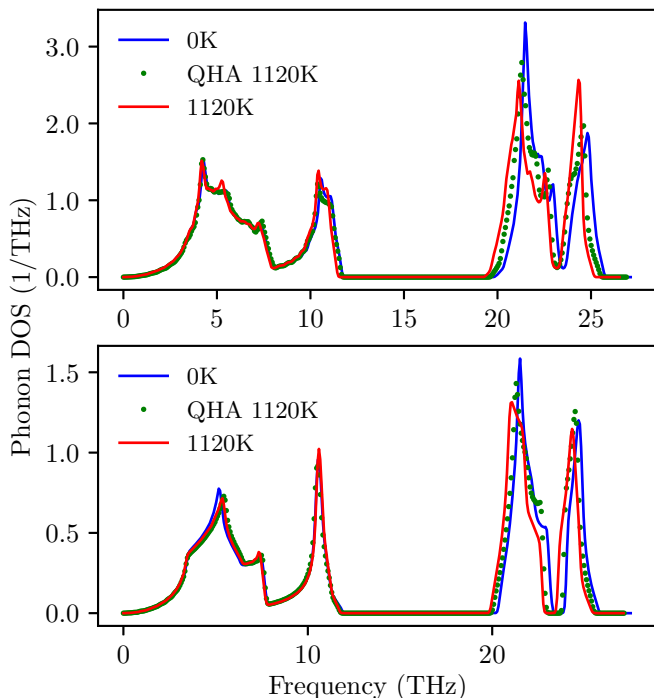


FIG. 7: Similar to Fig. 2, phonon DOS at 30 GPa for wurtzite (top) and zincblende (bottom) GaN at 0 K (blue), at 1120 K with the quasi-harmonic approximation (green dots), and at 1120 K by *s*-TDEP (red).

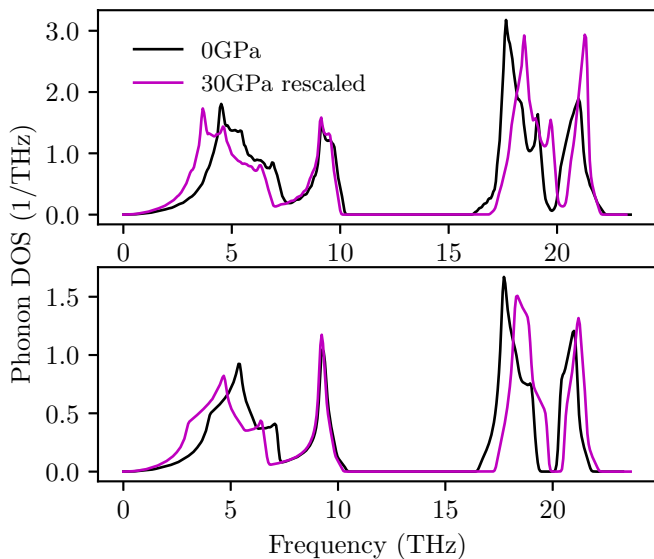


FIG. 8: Phonon DOS at 1120 K for wurtzite (top) and zincblende (bottom) GaN for 0 GPa (black) and 30 GPa with the mean frequency scaled to match that of the 0 GPa spectrum (magenta).

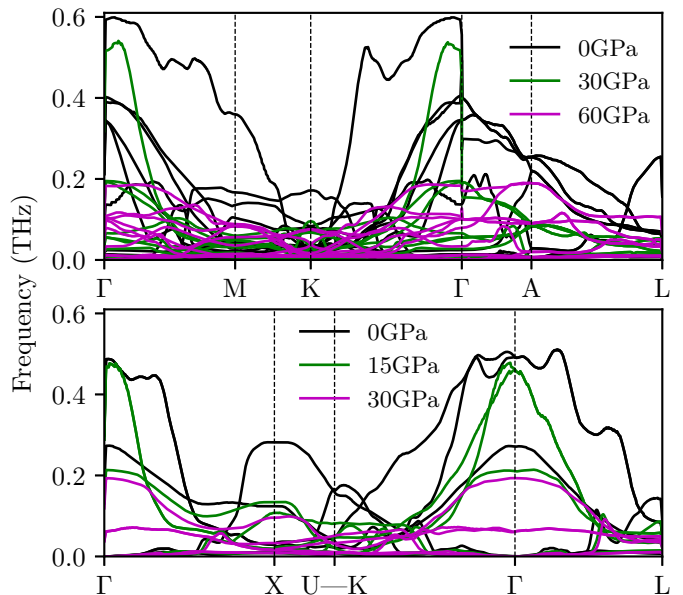


FIG. 9: Change in phonon linewidths between 0 K and 1120 K at three pressures for wurtzite (top) and zincblende (bottom) GaN. In each panel, pressure increases from the black to the green to the red curves.

thermal broadening in the wurtzite structure from Γ to A to L is largest at 0 GPa, smallest at 30 GPa, and returns to an intermediate values at 60 GPa. The phonon thermal broadening changes qualitatively with pressure, with all phonons undergoing a different nonlinear response.

B. Elastic constants and elastic instability

The universal elastic anisotropy index²⁸, A^U , was used to quantify the elastic anisotropy

$$A^U = \frac{G_V}{G_R} + \frac{K_V}{K_R} - 6, \quad (4)$$

where the subscripts R and V denote Reuss and Voigt averages, which provide lower and upper bounds, respectively, on the shear (G) and bulk (K) moduli. Using formulations summarized by Hill²⁹, Reuss and Voigt averages of the shear and bulk moduli were calculated using VASP elastic constants obtained from static lattices. (VASP determines the elastic tensor by applying finite distortions to a unit cell to determine stress-strain relationships.) Larger values of A^U indicate increasing elastic anisotropy, whereas $A^U = 1$ for an elastically-isotropic medium. Figure 10 shows that for both wurtzite and zincblende GaN, the elastic anisotropy first increases approximately linearly with pressure at low and moderate pressures. At high pressures, however, the elastic anisotropy increases rapidly, indicative of a pressure-induced lattice instability, *i.e.*, elastic collapse; this is shown in the Supplemental Information.

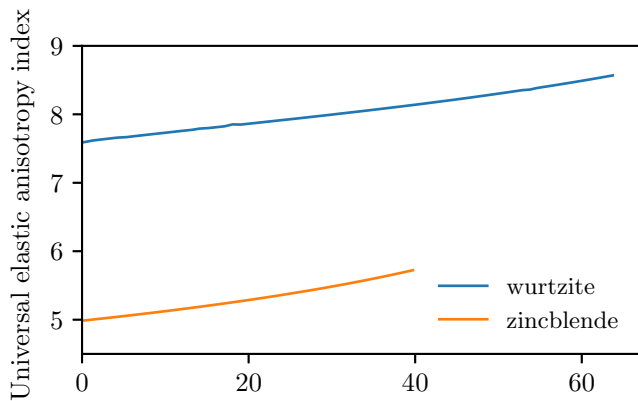


FIG. 10: The universal elastic anisotropy index A^U of wurtzite and zincblende GaN vs. pressure in the regime of elastic stability.

The pressures corresponding to the onset of elastic instabilities, P_{EI} , of zincblende and wurtzite GaN are identified by criteria similar to the “Born stability criteria”, but which account for finite pressures, as done previously.^{30–33} For cubic crystals such as zincblende, these elastic stability criteria are

$$B_{11} - B_{12} > 0, \quad B_{44} > 0, \quad B_{11} + 2B_{12} > 0. \quad (5)$$

For hexagonal crystals, such as wurtzite, they are

$$B_{11} > |B_{12}|, \quad B_{44} > 0, \quad B_{33}(B_{11} + B_{12}) > 2B_{13}^2. \quad (6)$$

In terms of the elastic constants C_{ij} and pressure P , the elastic stiffnesses, B_{ij} , are

$$B_{ii} = C_{ii} - P \text{ for } i = 1, 2, \dots, 6, \quad (7)$$

$$B_{1j} = C_{1j} + P \text{ for } j = 2, 3. \quad (8)$$

With increasing pressure, the first stability condition to fail is taken as the reason for an elastic instability. These conditions are explained further in the Supplemental Information. Using Eqs. 5 and 6, P_{EI} for the wurtzite and zincblende structures are found to be 65 and 40 GPa, respectively. Zincblende GaN becomes unstable when B_{12} exceeds B_{11} , *i.e.*, when the tetragonal shear modulus, $C_{11} - C_{12}$, becomes less than twice the pressure, $2P$. This is a “tetragonal shear instability.”³² Wurtzite GaN exhibits this same failure mechanism at 72 GPa, but first becomes elastically unstable when B_{44} becomes nonpositive, *i.e.*, when the pressure, P , exceeds C_{44} . The failures of these stability conditions are shown in Fig. 11.

These calculated values of P_{EI} fall within the range of approximately linear pressure dependence of the universal elastic anisotropy index (Fig. 10).

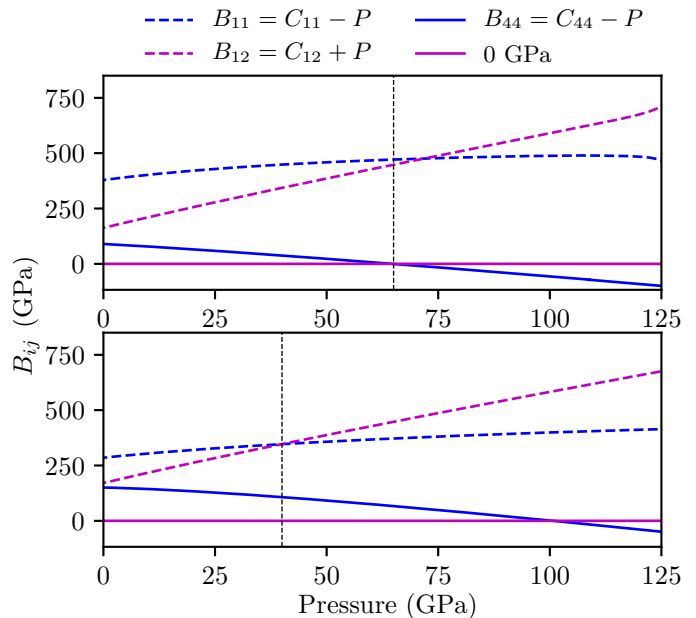


FIG. 11: Here we see elastic stiffnesses plotted against pressure. In both panels, B_{11} and B_{12} cross over where dashed blue and magenta lines intersect, and B_{44} is no longer greater than 0 GPa where solid blue and magenta lines intersect. Wurtzite GaN (top) becomes elastically unstable when B_{44} crosses the 0 GPa line at approximately 65 GPa; zincblende GaN (bottom) becomes elastically unstable when B_{11} and B_{12} cross over at 40 GPa. Vertical black lines identify P_{EI} .

IV. DISCUSSION

A. Pressure-temperature coupling and the quasiharmonic approximation

Mode Grüneisen parameters (Eq. 3) are found by evaluating the volume dependence of phonon frequencies, and Grüneisen parameters as in Fig. 6 are the basis for the quasiharmonic approximation (QHA). The quasiharmonic model assigns a temperature dependence of the phonon frequency to the thermal expansion β as

$$\omega_{i,\text{QHA}}(V, T_0 + \Delta T) = \omega_{i,0}(1 - \beta\gamma_i\Delta T), \quad (9)$$

where $\omega_{i,0}$ is the phonon frequency at the initial temperature T_0 , and γ_i is the mode Grüneisen parameter of Eq. 3. The phonon densities of states in both wurtzite and zincblende shift to lower frequencies (soften) with increasing temperature between 0 and 1120 K at fixed pressure. Figure 2 suggests that the quasiharmonic model may be adequate for understanding the temperature dependence of phonon thermodynamics at 0 GPa, although there are some differences compared to a more proper accounting of anharmonicity. The results of Fig. 7 suggest that the QHA for thermal shifts of phonons may be less reliable at higher pressures, however.

The s-TDEP method starts with quasiharmonic phonons for calculating the effective potential at elevated

temperature. Using a supercell with atoms displaced by these phonons, it obtains the best force constants for an ensemble of supercells. The s-TDEP method obtains anharmonic phonon frequency shifts (often attributed to the cubic and quartic terms in the phonon self-energy^{34,35}) by renormalizing^{21,22} the interatomic forces of Eq. 2 for the T and V of interest.

In general, phonon frequencies depend on the average positions of nuclei and temperature (which moves them about their average positions), so $\omega = \omega(V, T)$. The Grüneisen parameter is proportional to the volume derivative, $\gamma \sim (\partial\omega/\partial V)_T$, and the anharmonicity is proportional to the temperature derivative, $A \sim (\partial\omega/\partial T)_V$. By taking derivatives of these quantities with respect to the other variable, and equating mixed derivatives as $(\partial^2\omega/\partial T\partial V)_{VT} = (\partial^2\omega/\partial V\partial T)_{TV}$, it can be shown that the temperature derivative of the Grüneisen parameter $(\partial\gamma/\partial T)_V$ equals the volume derivative of the anharmonicity $(\partial A/\partial V)_T$. The physical origins of these two effects must be the same.

Figure 8 helps explain why the intrinsic anharmonicity changes with pressure. If the shape of the DOS did not change with pressure, the number of channels for three- and four-phonon processes would change only slightly, and in proportion to the mean phonon shift. Figure 8 shows that this is not the case because pressure causes a significant change in the shape of the DOS. Negative Grüneisen parameters cause the transverse acoustic modes to shift lower with respect to the mean, and the optical modes move higher. As these modes move apart with pressure, there are fewer three-phonon processes that can bridge them.

The resulting effects of pressure on explicit anharmonicity are evident in the phonon linewidths (which are, of course, zero in the QHA). Phonon linewidths are dominated by effects of cubic anharmonicity, since quartic anharmonicity gives no imaginary contribution to the phonon self-energy.^{34,35} Pressure-induced changes in three-phonon processes explain the pressure-driven differences in thermal phonon broadening seen in Fig. 9. At low or moderate temperatures, the line broadening of the optical modes $\omega(\mathbf{q})$ around the Γ point are dominated by down-conversion processes that have the kinematical factor

$$D_{\downarrow}(i, \mathbf{q}) = \frac{1}{N} \sum_{\mathbf{q}_1, \mathbf{q}_2, j_1, j_2} \Delta(\mathbf{q} - \mathbf{q}_1 - \mathbf{q}_2) \delta(\omega - \omega_1 - \omega_2), \quad (10)$$

where $\omega(\mathbf{q}_1)$ and $\omega(\mathbf{q}_2)$ are acoustic phonons. As pressure is increased, Fig. 5 shows that the optical modes shift upwards proportionally faster than the acoustic modes. The ratio of energies of the bottom of the optical modes to the top of the acoustic modes changes from approximately 1.55 at 0 GPa to 1.71 at 60 GPa for wurtzite, and changes from 1.61 at 0 GPa to 1.66 at 30 GPa for zincblende. If this were to reach 2.0, there would be zero terms in Eq. 10, but in three dimensions a change from 1.55 to 1.71 causes a large decrease in the number of

possible three-phonon processes around the Γ -point. The effects of cubic anharmonicity on the thermal linewidths should therefore be reduced strongly with pressure. The observed decrease in thermal broadening with increasing pressure is consistent with this, indicating a reduction in cubic anharmonicity from three-phonon processes. As thermal broadening decreases, harmonic phonons become better eigenstates of the system.

At temperatures of order 1000 K and pressures of order 10 GPa it is not appropriate to consider only a quasi-harmonicity $\propto P$, and an anharmonicity $\propto T$. These two contributions are not additive. The T -dependences of phonon frequency shifts and linewidths are pressure dependent; in other words, the effects of temperature and pressure on phonon frequencies have a coupling term $\propto TP$. Finally, the nonlinearity of the phonon shifts with pressure seen in Fig. 5 shows that a term proportional to P^2 may also be necessary to account for the phonon shifts at tens of GPa.

Both phonon frequency shifts and phonon linewidths are related to thermal conductivity. One implication of the failures of the QHA, and the anharmonicity at elevated T and P , is that calculations of thermal conductivity must be performed at the at high T and P of interest.

B. Elastic anisotropy and lattice instabilities

By calculating elastic anisotropy as a function of pressure, we showed that elastic anisotropy in both wurtzite and zincblende GaN increases with pressure. Both the zincblende and wurtzite structures of GaN become elastically unstable, and cannot exist at pressures higher than 40 and 65 GPa, respectively. Rocksalt is the thermodynamically favored structure of GaN at elevated pressures, with zincblende GaN predicted to transform to rocksalt GaN near 40 GPa, and wurtzite GaN observed to transform to rocksalt between 30 and 50 GPa. The predicted mechanism by which zincblende transforms to rocksalt begins with a tetragonal distortion¹, which is consistent with our result that zincblende GaN becomes elastically unstable due to tetragonal shear. A consensus in the literature is that wurtzite GaN forms a tetragonal intermediate structure prior to transforming to rocksalt. The work of Saitta, et al.⁸, implicate softening of the C_{44} and C_{66} elastic constants in this transformation. This is consistent with our work, where softening of C_{44} and C_{66} with increasing pressure lead to failures of two elastic stability conditions in wurtzite GaN at 65 and 72 GPa, respectively.

Our result that elastic instability occurs at 65 and 40 GPa in wurtzite and zincblende GaN, respectively, places upper bounds on the existence of these structures. In discussing the transformation pathway of wurtzite to rocksalt in AlN, InN, and GaN, one author ruled out the metastability of the wurtzite structure above the transformation pressure for AlN and InN, but not for GaN.³ This same work calculated a coexistence pressure of 74

GPa for the SC16 and wurtzite structures of GaN, suggesting the possibility of wurtzite metastability up to at least 74 GPa. Our work shows that by 65 GPa, wurtzite GaN will be mechanically unstable, preventing such a thermodynamic metastability. Similarly, above 40 GPa, zincblende GaN will no longer be thermodynamically metastable.

The phonon dispersion relations of GaN indicate that these results on elastic anisotropy and elastic stability of wurtzite and zincblende GaN should not be significantly dependent on temperature.

In the long wavelength limit, the elastic constants may be determined as a function of force constants. Given this relationship between elastic constants and force constants, invariance of low-energy acoustic phonon branches equates to invariance of the elastic constants. In Fig. 3, we see that the low-energy acoustic phonon modes are not sensitive to temperature; in particular, we see in Fig. 3 that the red and blue curves in each panel overlap nearly perfectly when the acoustic branches extending from the Γ point are linear. (As shown in the Supplemental Information, the low-energy acoustic modes are insensitive not only to the full effects of temperature but also to the temperature-driven volume changes between 0 and 1120 K.) Similarly we see in Fig. 2 that the phonon DOS at 0 and 1120 K overlap nearly perfectly below about 5 THz in both structures of GaN. As the elastic constants of either structure do not change significantly with temperature, temperature will not significantly alter the pressures at which these structures become elastically unstable, or the elastic anisotropy trends at 0 K.

V. CONCLUSIONS

For a pressure of 0 GPa, a simple quasiharmonic approximation, which attributes both temperature and pressure dependences of phonon self-energies to changes in volume, predicts temperature dependences of phonons in wurtzite and zincblende GaN that are approximately correct. Effects of the explicit anharmonicity of phonons

varies with pressure, and our results suggest a quasiharmonic approximation predicts thermal shifts of phonons less successfully by 30 GPa.

Pressure determines the degree to which temperature alters the lifetimes of optical phonons, owing to a decrease in the number of 3-phonon downscattering channels for optical modes. Accounting for the effects of T and P on the phonons in both zincblende and wurtzite GaN over a range of T and P of approximately 1000 K and tens of GPa requires, at a minimum, that phonon frequencies have terms that depend on P (quasiharmonicity), T (explicit anharmonicity), PT , and P^2 .

The elastic anisotropy was found to increase with pressure in both wurtzite and zincblende GaN. An elastic instability was found in wurtzite GaN at 65 GPa and in zincblende GaN at 40 GPa, providing upper bounds for the possible metastability of either phase, after rock-salt GaN becomes thermodynamically favorable. Thermal trends in long-wavelength phonons show that the pressures of elastic instability should be reliable to temperatures of 1120 K.

VI. ACKNOWLEDGEMENTS

We thank Sacha Verweij and Nina Shulumba for useful conversations that informed this work.

We are grateful for the use of resources at the National Energy Research Scientific Computing (NERSC) Center, a DOE Office of Science User Facility supported by the Office of Science of the U.S. Department of Energy under Contract No. DE-AC02-05CH11231, without which this work would not have been possible.

This work was funded by the Department of Energy both through the Carnegie-DOE Alliance Center's Stewardship Sciences Academic Alliance Program, and through the Office of Science Graduate Fellowship Program (DOE SCGF), made possible in part by the American Recovery and Reinvestment Act of 2009, administered by ORISE-ORAU under Contract No. DE-AC05-06OR23100

¹ M. Wilson and P. A. Madden, *Journal of Physics: Condensed Matter* **14**, 4629 (2002).
² T. Lei, M. Fanciulli, R. J. Molnar, T. D. Moustakas, R. J. Graham, and J. Scanlon, *Applied Physics Letters* **59**, 944 (1991).
³ J. Serrano, A. Rubio, E. Hernández, A. Muñoz, and A. Mujica, *Physical Review B* **62**, 16612 (2000).
⁴ H. Xia, Q. Xia, and A. L. Ruoff, *Phys. Rev. B* **47**, 12925 (1993).
⁵ A. Mujica, A. Rubio, A. Muñoz, and R. J. Needs, *Reviews of Modern Physics* **75**, 863 (2003).
⁶ M. D. Knudson, Y. M. Gupta, and A. B. Kunz, *Phys. Rev. B* **59**, 11704 (1999).
⁷ A. Zaoui and W. Sekkal, *Physical Review B* **66**, 174106

(2002).
⁸ A. M. Saitta and F. Decremps, *Phys. Rev. B* **70**, 035214 (2004).
⁹ C. W. Li, X. Tang, J. A. Muñoz, J. B. Keith, S. J. Tracy, D. L. Abernathy, and B. Fultz, *Phys. Rev. Lett.* **107**, 195504 (2011).
¹⁰ L. Mauger, J. E. Herriman, O. Hellman, S. J. Tracy, M. S. Lucas, J. A. Muñoz, Y. Xiao, J. Li, and B. Fultz, *Phys. Rev. B* **95**, 024308 (2017).
¹¹ N. Shulumba, Z. Raza, O. Hellman, E. Janzén, I. A. Abrikosov, and M. Odén, *Phys. Rev. B* **94**, 104305 (2016).
¹² W. Kohn and L. J. Sham, *Physical Review* **140** (1965).
¹³ G. Kresse and J. Furthmüller, *Physical Review B* **54**, 11169 (1996).

- ¹⁴ G. Kresse and J. Furthmüller, *Computational Materials Science* **6**, 15 (1996).
- ¹⁵ P. E. Blöchl, *Physical Review B* **50**, 17953 (1994).
- ¹⁶ H. Monkhorst and J. Pack, *Physical Review B* **13**, 5188 (1976).
- ¹⁷ O. Hellman, I. A. Abrikosov, and S. I. Simak, *Phys. Rev. B* **84**, 180301 (2011).
- ¹⁸ O. Hellman and I. A. Abrikosov, *Physical Review B* **88**, 144301 (2013).
- ¹⁹ O. Hellman, P. Steneteg, I. A. Abrikosov, and S. I. Simak, *Physical Review B* **87**, 104111 (2013).
- ²⁰ N. Shulumba, O. Hellman, and A. J. Minnich, *Phys. Rev. B* **95**, 014302 (2017).
- ²¹ M. L. Klein and G. K. Horton, *Journal of Low Temperature Physics* **9**, 151 (1972).
- ²² D. J. Hooton, *The London, Edinburgh, and Dublin Philosophical Magazine and Journal of Science* **46**, 422 (1955).
- ²³ X. Gonze, J.-C. Charlier, D.-C. Allan, and M.-P. Teter, *Phys. Rev. B* **50**, 13035 (1994).
- ²⁴ X. Gonze and C. Lee, *Phys. Rev. B* **55**, 10355 (1997).
- ²⁵ S. Biernacki and M. Scheffler, *Physical Review Letters* **63**, 290 (1989).
- ²⁶ G. D. Barrera, J. A. O. Bruno, T. H. K. Barron, and N. L. Allan, *Journal of Physics: Condensed Matter* **17**, 217 (2005).
- ²⁷ L. Wang, P. F. Yuan, F. Wang, Q. Sun, Z. X. Guo, E. J. Liang, and Y. Jia, *Materials Chemistry and Physics* **148**, 214 (2014).
- ²⁸ S. I. Ranganathan and M. Ostoja-Starzewski, *Phys. Rev. Lett.* **101**, 055504 (2008).
- ²⁹ R. Hill, *Proceedings of the Physical Society. Section A* **65**, 349 (1952).
- ³⁰ J. Wang, S. Yip, S. Phillpot, and D. Wolf, *Physical Review* **71**, 4182 (1993).
- ³¹ J. Wang, J. Li, S. Yip, S. Phillpot, and D. Wolf, *Physical Review B* **52**, 12 627 (1995).
- ³² B. B. Karki, G. J. Ackland, and J. Crain, *Journal of Physics: Condensed Matter* **9**, 8579 (1997).
- ³³ G. V. Sin'ko and N. A. Smirnov, *Journal of Physics: Condensed Matter* **14**, 6989 (2002).
- ³⁴ D. C. Wallace, *Thermodynamics of Crystals* (Dover Publications, 1972).
- ³⁵ A. A. Maradudin and A. E. Fein, *Physical Review* **128**, 2589 (1962).